PCCP

RSC Publishing

PERSPECTIVE

View Article Online
View Journal | View Issue

Published on 20 May 2013. Downloaded by University of Science and Technology of China on 10/07/2013 12:30:27.

STM tip-assisted single molecule chemistry

Aidi Zhao, Shijing Tan, Bin Li, Bing Wang,* Jinlong Yang and J. G. Hou*

Cite this: *Phys. Chem. Chem. Phys.*, 2013, **15**, 12428

Scanning tunnelling microscopy (STM) has been a unique and powerful tool in the study of molecular systems among various microscopic and spectroscopic techniques. This benefits from the local probing ability for the atomically resolved structural and electronic characterization by the STM tip. Moreover, by using the STM tip one can modify a given structure and thus control the physical and chemical properties of molecules at a single-molecule level. The rapid developments in the past 30 years have extended the functions of STM far beyond characterization. It has shown the flexibility to combine STM with other techniques by making use of the advantages of the STM tip, demonstrating important applications in the growing nanotechnology. Here we review some recent progresses in our laboratory on single molecule chemistry by taking advantage of tip-assisted local approaches, such as the identification of specific orbitals or states of molecules on surfaces, tip-induced single-molecule manipulation, atomically resolved chemical reactions in photochemistry and tip-induced electroluminescence. We expect more joint techniques to emerge in the near future by using the unique advantages of STM tip, providing more powerful tools for the growing requirements of new materials design and the mechanism of chemical reactions at the molecular scale.

Received 5th April 2013,
Accepted 17th May 2013

DOI: 10.1039/c3cp51446c

www.rsc.org/pccp

1. Introduction

Since the first scanning tunnelling microscope was invented in 1982 by G. Binnig and H. Roher,[1,2] it has been a powerful tool in real-space imaging of surface structures, especially for its atomic resolution, as well as its capabilities in the characterization of the electronic properties of nanostructures. In the past 30 years, techniques based on scanning tunnelling microscopy (STM) have developed rapidly. Today, scanning probe microscopy has become a big family and has been widely used in physics, chemistry, material science, and biology. In this Perspective, we mainly focus on the results obtained in our laboratory on the characterization and manipulation of single molecules adsorbed on various substrates, in particular, on the role of the STM tip. Some recent progresses on the tip-induced electroluminescence and the tip-assisted chemical reactions at

Hefei National Laboratory for Physical Sciences at the Microscale (HFNL), University of Science and Technology of China (USTC), Hefei, Anhui 230026, P. R. China. E-mail: bwang@ustc.edu.cn, jghou@ustc.edu.cn

Aidi Zhao

Aidi Zhao is an Associate Professor at the University of Science and Technology of China (USTC). He received his PhD in Condensed Matter Physics in 2006 from USTC under the supervision of Prof. J. G. Hou. He has been studying physical and chemical properties of single molecules and low-dimensional materials by using low-temperature scanning tunnelling microscopy since 2001. His current research interests include single-molecule chemistry/physics, graphene physics, and thin-film physics.

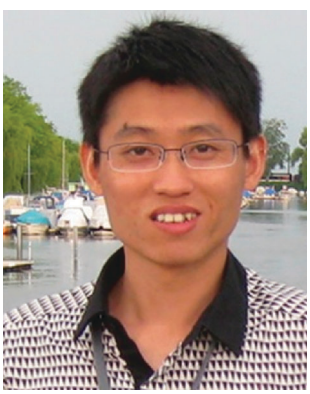

Shijing Tan

Shijing Tan received his PhD from USTC in 2012 under the supervision of Prof. Bing Wang and Prof. J. G. Hou. He has been studying molecular level chemical reactions of water, methanol, oxygen and carbon dioxide on the photocatalyst TiO_2 surface with scanning tunnelling microscopy since 2006. In 2012, He joined Prof. Yi Luo's group at KTH Royal Institute of Technology as a postdoctoral fellow, where he continues his study on the mechanism of photo-oxidation of water and methanol on TiO_2 surface.

This journal is © the Owner Societies 2013

Published on 20 May 2013. Downloaded by University of Science and Technology of China on 10/07/2013 12:30:27.

a single-molecule level are also included. These efforts demonstrate the capability and feasibility of the combination of STM with other techniques, which may extend to much wider applications of STM for the understanding of microscopic physical processes at a fundamental level by making use of the unique advantages of the STM tip.

2. Characterization of specific molecular orbitals and densities of state

Because of its probing ability of local structures and electronic properties, STM has been widely used to characterize molecular systems, such as the structures of molecular assemblies,[3–6] the conformation/chirality[7,8] and orientations[9] of single molecules, the electronic transport of molecular films and single molecules,[10] the vibrational properties of single molecules,[11,12] *etc.* Such progresses have pushed the applications of STM to a high level far beyond simple structural and electronic characterization. However, in principle, STM does not provide direct information on chemical resolution. Although some other macroscopic techniques may provide chemical resolution, in most cases these techniques become less sensitive when only a few molecules or even single molecules are concerned, and it is difficult to obtain high spatial resolution. In the current studies of molecular electronics and microscopic processes of chemical reactions, it is of great importance to identify different molecular species or reaction products. We show here that in some cases, STM can be utilized to distinguish chemical species adsorbed on surfaces, and to detect specific electronic states and molecular orbitals.

2.1 Characterization of different species on oxide surfaces

The rutile TiO_2(110) is a model system in the study of catalytic and photocatalytic chemical reactions on oxide surfaces.[13–21] There exist commonly intrinsic defects of oxygen vacancies (O_V) and impurities of the hydroxyl group (OH_b) (Fig. 1a). It is known that the O_V and OH_b are both present as bright protrusions in the empty state images, as shown in Fig. 1b. Although in most cases, the OH_b is observed a little brighter than the

Bin Li

Bin Li received his PhD in physics from University of Science and Technology of China (USTC) in 2002 under the supervision of Prof. Jian Guo Hou. He had then worked as a postdoc in Prof. C. T. Chan's group at the Hong Kong University of Science and Technology, and as a visiting scholar in Prof. W. T. Yang's group at Duke University. From 2005, he has been an Associate Professor at USTC. His research interests include density functional theory, STM simulation, and field emission modeling.

Bing Wang

Bing Wang, Professor of Physics. He received his PhD in Condensed Matter Physics from USTC in 1995. His main research interests focus on the physics and chemistry of low-dimensional materials at the molecular level.

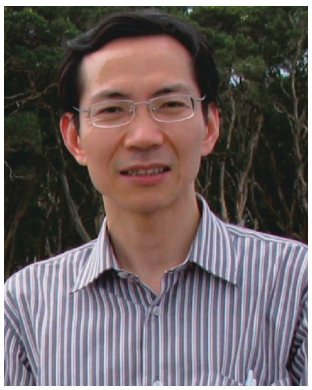

Jinlong Yang

Jinlong Yang, currently a Changjiang Professor of Chemistry, Dean of the School of Chemistry and Material Sciences of USTC, received his PhD in Condensed Matter Physics from USTC in 1991. He is the recipient of the Young Chemist Award from the Chinese Chemical Society and the National Award (grade two) for natural science, and is the supervisor of two authors of the National Excellent Doctoral Thesis Award. His interests focus on developing first principles methods and their application to clusters, nano structures, solid materials, surfaces and interfaces.

J. G. Hou

J. G. Hou (Jianguo Hou) is Professor of Physics and Chemistry at USTC. He is Academician of the Chinese Academy of Science, Fellow of the Third World Academy of Science, President of the Chinese Vacuum Society and President of USTC. He received his PhD in Condensed Matter Physics from USTC in 1989. He is the recipient of the National Award (grade two) for natural science, Ho Leung Ho Lee, Qiushi, and Tan Kan Kee Awards. His main research interests focus on the physics and chemistry of low-dimensional materials on the molecular level.

Published on 20 May 2013. Downloaded by University of Science and Technology of China on 10/07/2013 12:30:27.

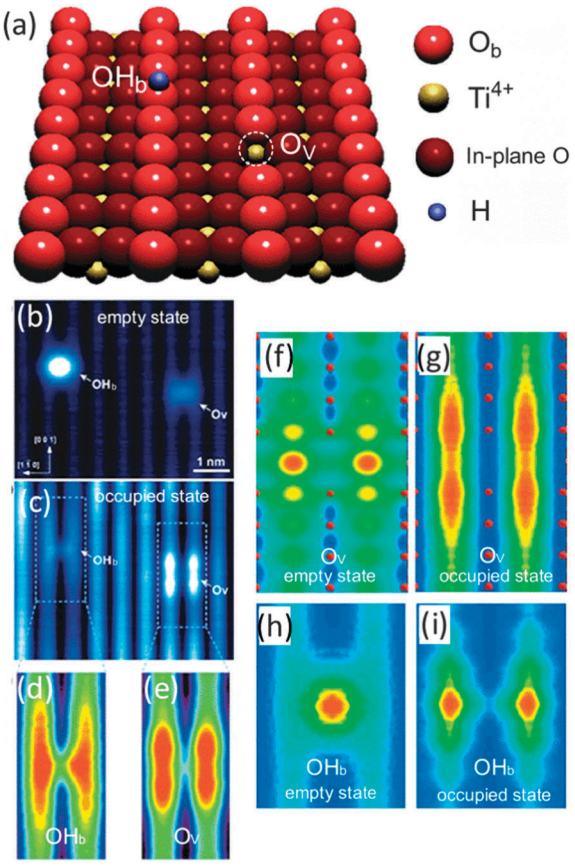

Fig. 1 Characterization of O_V and OH_b on a TiO_2(110)-1×1 surface. (a) Structural model of a TiO_2(110)-1×1 surface with O_V and OH_b. (b and c) Empty state (1.4 V, 10 pA) and occupied state (−1.4 V, 5 pA) STM images of a TiO_2(110)-1×1 surface with O_V and an OH_b. Size: 5.8 × 6.6 nm^2. (d and e) Magnified high-contrast occupied state images of OH_b and O_V, respectively. (f and g) Theoretically simulated STM images of O_v at 1.0 V (empty state) and −1.1 V (occupied state), respectively; (h and i) Theoretically simulated STM images of OH_b at 1.0 V (empty state) and −1.4 V (occupied state), respectively. (Modified with permission from ref. 37. Copyright 2009 American Institute of Physics.)

O_V,[17,22,23] the apparent heights of both the OH_b and O_V are dependent on the imaging conditions.[24,25] It may sometimes be misleading to identify these two species just from the protrusions in the empty state images. These two defects introduce excess electrons into the unoccupied 3d orbital of the neighbouring Ti atoms, which may affect significantly the physical and chemical properties of TiO_2 surfaces, such as the ability to chemisorb electron accepting or donating molecules and surface electron transport.[26–34] The excess charge was observed as a broad peak at around 0.9 eV below the Fermi level in photoelectron and electron energy loss spectroscopy of a reduced TiO_2 surface.[35,36] However, the spatial distributions of the excess charge also provide important information for the molecular adsorption and chemical reactions. By using atomic-resolved STM, the spatial distribution of the occupied Ti 3d states on reduced TiO_2 surfaces can be seen in the occupied state image.[37] We find that the occupied state images can give distinguishable features between the OH_b and the O_V.[37] As shown in Fig. 1c, when the area was imaged with a negative bias voltage of −1.4 V and a low current of 5 pA, the O_V and the OH_b group give different contrast at the nearby Ti^{4+} sites. The high-contrast occupied-state images of the OH_b and O_V in Fig. 1d and e show a similar symmetric bright four-lobed appearance around the defects and each lobe is extended over several Ti^{4+} sites. These observations suggest the excess charges of O_V and OH_b are both delocalized and spread over the near Ti^{4+} sites. However, the detailed distributions of O_V and OH_b are still different. The OH_b is present as a shuttle-like shape, while the O_V is a dumbbell shape. Theoretical simulated empty and occupied state STM images of O_V and OH_b in Fig. 1f–i are very consistent with the experimental observations, which confirms the different features especially in the occupied state image, although both of the defects show that the Ti 3d density of states (DOS) transfers to several proximate Ti^{4+} sites. Such character of the delocalized charge distribution has affected the site-specific chemical activity of the reduced TiO_2(110)-1×1 surfaces. For example, it is observed that the adsorption behaviours of CO are strongly dependent on the delocalized charge distribution of O_V.[38]

Since OH_b defects commonly exist on TiO_2 surfaces, and many of the reactions also involve H, it is thus quite important to identify the OH_b groups from other species. The method by characterizing the occupied state image shown in Fig. 1 is not always practical. Alternatively, one may detect the OH_b groups by applying a voltage pulse to dehydrogenate OH_b groups using the STM tip.[22,23] However, such a method is destructive and may cause damage of the molecules concerned. A more practical way can be used by changing the imaging conditions. It is found that the contrast of OH_b is significantly dependent on the distance of the STM tip from the OH_b.[24] Fig. $2a_1$ shows an image of a TiO_2(110) surface with coexistence of O_V and OH_b, acquired at 1.2 V and 3 pA. With the increase of tunnelling current to 700 pA, the OH_b species become almost invisible, meanwhile the contrast for O_V becomes much obvious, as shown in Fig. $2a_2$. When the tunnelling current is set back to 3 pA, the contrast of OH_b is recovered, as shown in Fig. $2a_3$. A similar contrast change can be observed by adjusting the bias voltage to vary the tip–sample distance. The theoretical calculations suggest that the contrast-dependence of OH_b on the tip–sample distance is because of the electric field change, which may cause O–H bond bending under a high enough electric field when the tip–sample distance is reduced, as shown in Fig. $2b_1$–b_3. Such a feature of OH_b under variation of the tip–sample distance can be used more easily to identify OH_b groups on rutile TiO_2(110) surface when the OH_b species is involved, as shown in ref. 39.

2.2 Characterization of specific states of single molecule

Besides STM imaging, scanning tunnelling spectroscopy (STS) is used to study the local electronic structure of a sample by measuring the *I*–*V* curves of the tunnelling junction. According to the principle of STM, the d*I*/d*V* signal is proportional to the local density of states (DOS) if a constant DOS of the tip is considered.[40] The d*I*/d*V* spectra and maps can be obtained simultaneously with *I*–*V* measurements and constant-current

 This journal is © the Owner Societies 2013

Published on 20 May 2013. Downloaded by University of Science and Technology of China on 10/07/2013 12:30:27.

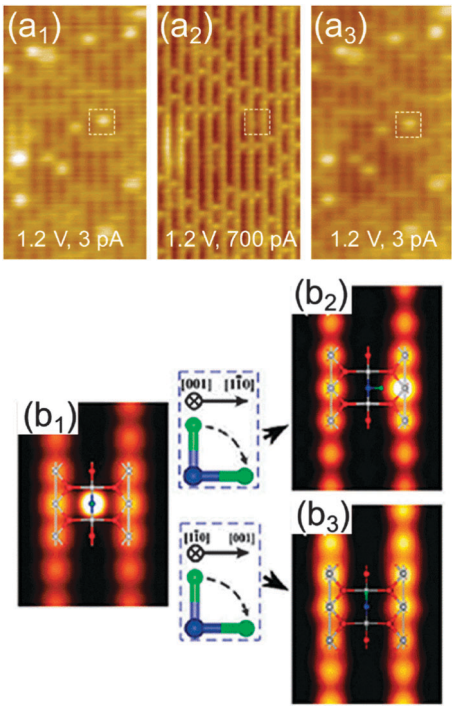

Fig. 2 Dependence of OH_b contrast on the tip–sample distance. (a_1–a_3) STM images of the partially hydroxylated TiO_2(110)-1×1 surface within the same area at various imaging conditions. Size: 7.1×14 nm^2. (b_1–b_3) Simulated empty state STM images with superposed ball–stick models for normal orientated OH, parallel orientated OH along the [1$\bar{1}$0] direction, and parallel orientated OH along the [001] direction, respectively. (Modified with permission from ref. 24. Copyright 2009 American Chemical Society.)

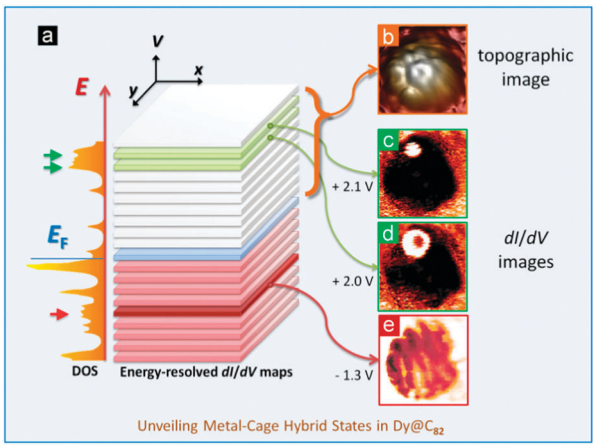

Fig. 3 Unveiling intramolecular metal–cage hybrid states in single Dy@C_{82} molecules. (a) Left: DOS of Dy@C_{82}, right: schematic drawing illustrating the d*I*/d*V* maps within small energy widows, reflecting an energy-resolved spatial distributions of electronic states of a single Dy@C_{82} molecule. (b) An ordinary constant-current topographic image giving the integral signal of all energy windows from the E_F to the applied voltage. (c)–(e) d*I*/d*V* maps recorded at +2.1 V, +2.0 V and −1.3 V, respectively, showing the hybrid states of metal–cage at certain energies [(c) and (d)]. (Modified with permission from ref. 44. Copyright 2003, American Physical Society.)

imaging respectively by applying a small modulation to the bias voltage. The d*I*/d*V* mapping makes it possible to image the real-space distribution of electron states at a specific energy. It has been employed to study the quantum scattering pattern of confined surface electrons,[41] the local impurity states in high-temperature superconductors,[42] molecular orbitals of individual molecules,[43–45] *etc.*

An early work by Wang *et al.*[44] shows that the d*I*/d*V* mapping helps to unveil the intramolecular metal–cage hybrid states in single Dy@C_{82} molecules. To reveal the endohedral atom or cluster in the fullerene cage is a challenging task since the carbon cage acts as a Faraday cage. The Dy@C_{82} molecule has a Dy atom encapsulated in a C_{82} fullerene cage. It has been a long-term desire to characterize the location of the internal atom in such an endohedral metallofullerene. The ordinary STM images would not help in solving this problem because they could only give overall topographic information of the carbon cage. However, by performing the d*I*/d*V* mapping, one is able to map spatially the distribution of the on-cage hybrid states. These specific states reflect the orbital hybridization and charge transfer for the interaction between the Dy atom and the C_{82} cage and hence project the metal location. The working principles are illustrated in Fig. 3. The energy-resolved d*I*/d*V* images provide the distribution of d*I*/d*V* signals in the *x*–*y* plane of a small voltage window (horizontal layers in Fig. 3a), which direct reflect the distribution of the DOS in a small energy window. Fig. 3b shows an ordinary STM image exhibiting the topographic structure of the C_{82} cage. By recording a series of images in different energy windows, we found strongly protruded features in d*I*/d*V* maps recorded at around +2 V (Fig. 3c and d). These features reflect the metal–cage hybrid states show up in DOS as indicated by green-coloured arrows (left panel in Fig. 3a). The d*I*/d*V* maps at other bias voltages show only cage-related features, for example, recorded at −1.3 V as shown in Fig. 3e. This example shows that the STM can even unveil the electronic states and intramolecular structures in such complicated molecules. There has been a number of reports concerning the microscopic study of intramolecular states in endohedral fullerene molecules.[46–51] For example, Huang *et al.*[47] observed the intramolecular switch based on tunnelling electron-driven rotation of the triangular Sc_3N cluster within an icosahedral C_{80} fullerene cage adsorbed on a Cu(110)–O surface. The geometric configuration of the cluster leads to detectable differences in the topological STM images of the molecule, indicating that the cluster also contributes to the state of the fullerene cage. Grobis *et al.*[46] reported the spatial distribution of elastic and inelastic tunnelling in single Gd@C_{82} molecules adsorbed on Ag(001) and found the dominant inelastic channel is spatially well localized to a particular region of the molecule. However, they did not observe Gd-related states in their experiment. One possible factor can be attributed to the substrate. The Gd@C_{82} molecules deposited on the Ag surface have been shown to suffer strong charge transfer from the substrate. This charge transfer was estimated to be as much as 1 electron per molecule and might influence greatly the electronic state of the cage. Another possibility is that the molecular orientation plays a crucial role in detecting metal–cage hybrid states. In all of the experimental d*I*/d*V* maps

Published on 20 May 2013. Downloaded by University of Science and Technology of China on 10/07/2013 12:30:27.

in our study, the metal atom is found to be on the side of the cage, suggesting that the Dy@C_{82} molecules adsorbed on the substrate are in a small subset of all of the possible orientations. The metal–cage hybrid states can be readily detected with STM in this subset of orientations.

2.3 Tip-assisted characterization of electronic states in single molecules

In the instances mentioned above, an ordinary W tip was used for the experiments. Here we show that specially-prepared tips may play an important role in single-molecule characterization. The principle of STM imaging relies on the coupling between electron wavefunctions of the tip and the sample. In most cases, one needs to know the physical and chemical properties of the tip. Various works have shown the importance of the tip in STM experiments.[52–56] In general, a tungsten tip has an s-orbital-like wavefunction with a flat DOS at its apex,[40] which can provide the information dominantly from the sample itself. However, some sample states are difficult to detect with a "normal" tungsten tip due to very weak coupling between the sample and tip because of their wavefunction mismatching.[53,57] This puts forward a need to decorate or functionalize the STM tip.[58–61] In the cases of the adsorbed molecules on metal surfaces, various local electronic hybrid states can be introduced due to the interaction of molecule orbitals with nonlocal electronic bands and local atomic orbitals of the metal substrates.[62,63] These states at the molecule–metal interface are speculated to be crucial in functional molecular devices. However, this kind of elusive molecule–surface hybrid (MSH) state is hard to detect by conventional spectroscopic techniques.

For instance, we have shown that the MSH states in single molecules on a metal surface can be detected directly with STM by employing a specific tip[63] due to the extended spatial distribution of the frontier orbital in the tip. It is observed that an ordinary W tip and an Fe-coated W tip (Fe/W tip) give quite similar patterns for the cobalt phthalocyanine (CoPc) molecules on a Au(111) surface in the occupied state images (Fig. 4a and b). However, the dI/dV curves in the STS measurements with the two tips at the centre of CoPc molecule exhibit quite different features in the negative bias voltages (Fig. 4c and d). Four tunnelling resonances were observed at about −0.1 (TS_1), −0.4 (TS_2), −0.75 (TS_3), and −1.35 (TS_4) V when the Fe/W tip was used to acquire the dI/dV curves. However, only three tunnelling resonances were observed when the bare W tip was used. The resonance TS_2 was absent in the latter case. Combining the dI/dV map and theoretical analysis we found that the states at the energies of the resonances TS_1, TS_3 and TS_4 have larger components localized on the Co ion, while the state at the energy of the resonance TS_2 is of the MSH state, which is delocalized around the central Co ion. This delocalization can be seen from the dI/dV maps of the molecule at −0.4 V (Fig. 4e), whereas the dI/dV map at the same bias obtained with a W tip does not show such a feature (Fig. 4f). Further analysis reveals the mechanism of MSH state detection by the Fe/W tip instead of a bare W tip by taking account of the spatial distribution of the frontier orbitals of both tips as well as the MSH state.

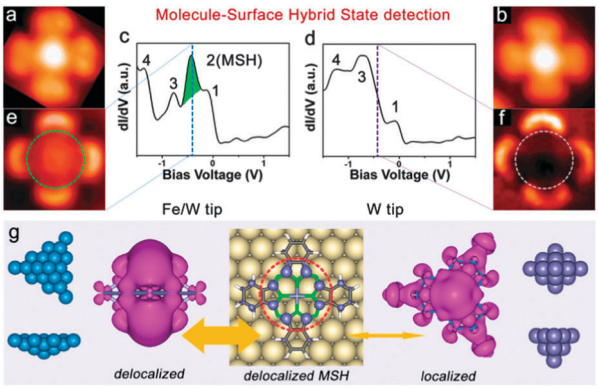

Fig. 4 MSH state detection with STM. (a and b) STM topographic images (−1.3 V, 0.4 nA) of CoPc on Au(111) obtained with a W tip and Fe/W tip, respectively. (c and d) The STS of CoPc on Au(111) measured with an W tip and a Fe/W tip at the molecule centre, respectively. (e and f) dI/dV maps at a sample bias of −0.4 V with an W tip and Fe/W tip, respectively. (g) Theoretically simulated LUMO+1 of the Fe/W tip, and LUMO of the W tip show delocalized and localized features respectively. The simulated delocalized MSH state of the CoPc molecule also exhibits a delocalized feature, matching the LUMO+1 of the Fe/W tip. (Modified with permission from ref. 63. Copyright 2008, American Chemical Society.)

Fig. 4g shows that the lowest unoccupied molecular orbital (LUMO) of the W tip is found to be s-orbital-like, but the LUMO+1 of Fe/W tip is identified as a more delocalized d_{yz}-derived state and is ascribed to be responsible for MSH state detection. That is to say, the conventional W tip cannot detect the states at the energy of the resonance TS_2 due to weak spatial matching between the localized s-like LUMO of the W tip and nonlocal MSH state, whereas the similar delocalized properties of the LUMO+1 of the Fe/W tip and the MSH state bring their good wavefunction matching, resulting in the strong tunnelling resonance TS_2. This work demonstrates the importance of the elaborate tip on single-molecule characterization and emphasizes the capability of STM in detecting elusive MSH states at a single-molecule level.

The importance of the tip condition is manifested by another example.[64] It is found that the spatial symmetry matching of the orbitals between the tip and the molecule can lead to the distinct transport properties of single molecules. Negative differential resistance (NDR) devices consisting of only one or a few molecules have been pursued for a long time. Although several different NDR mechanisms were demonstrated,[65–70] the role of the symmetry-matching of orbitals between electrodes was not examined. Considering the nature of the d orbitals of the Co^{2+} ion of a CoPc molecule, we used Ni single crystal tips to measure the electronic transport of CoPc molecules, as shown in Fig. 5a and b. An apparent NDR effect is observed in the I–V curve (curve A in Fig. 5b) at the negative bias voltage, with a maximum current (I_{max}) at −0.87 V and a minimum current (I_{min}) at −1.34 V, respectively. The NDR effect vanishes gradually when the tip is moved off the Co ion (curve B and C). Under the same experimental conditions we repeated the measurements with the conventional W tip; the obtained I–V curve exhibits ordinary monotonic behaviour.

 This journal is © the Owner Societies 2013

Published on 20 May 2013. Downloaded by University of Science and Technology of China on 10/07/2013 12:30:27.

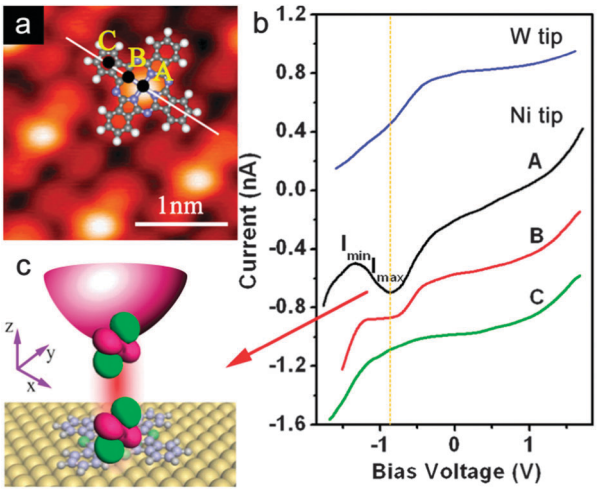

Fig. 5 NDR from orbital-symmetry matching between tip and molecule. (a) STM topographic image (−0.7 V, 0.2 nA) of CoPc monolayer on Au(111), with a CoPc ball-stick sketch superimposed on one molecule. (b) *I–V* curves measured with a Ni tip (1.2 V, 0.2 nA) over sites A, B, and C, and with a W tip (−1.0 V, 0.4 nA) over site A. The curves are shifted vertically for clarity. (c) The schematic drawing showing the local orbital symmetry matching between the tip and the molecule. (Modified with permission from ref. 64. Copyright 2007, American Physical Society.)

Detailed analysis indicates that the NDR effect in the Ni-tip/CoPc-molecule undergoes a novel mechanism in which local orbital symmetry matching between the Ni tip and Co atom plays a crucial role. The Ni single-crystal tip has well-defined $d_{yz(xz)}$ orbitals that completely dominate in the DOS of the tip and exhibit a sharp spectral profile at 0.23 eV, while the DOS of the W tip has a smooth distribution in a large energy window of empty states. On the other hand, the DOS of the Co ion in CoPc exhibits a prominent peak at −0.69 eV originating from the $d_{xz(yz)}$ orbitals. When the sample bias voltage sweeps through −0.9 V, the $d_{yz(xz)}$ orbitals at the Ni tip match maximally the $d_{xz(yz)}$ orbitals of the Co ion in both energy and spatial symmetry, leading to a giant tunnelling matrix element and hence the enhanced tunnelling current observed in the *I–V* curve (Fig. 5c). This work demonstrates a new mechanism for NDR by employing spatial discreteness instead of conventional energy discreteness to control the electronic transport through the device.

3. STM tip-assisted functionalization and reaction of single-molecules

Even in the very beginning of STM development, scientists already realized the ability of STM for real-space manipulation of individual atoms and molecules. Early studies showed the ability of STM to move single molecules and atoms by directly using the STM tip as a nano finger. The first instance of manipulating single molecules is demonstrated by Foster *et al.*[71] in 1989. They reported the reversible pinning and removal of individual organic molecules to a graphite surface by applying a voltage pulse to the sample. Although they did not give a mechanism, this pioneering work showed the capability of STM to manipulate single molecules of only a few angstroms and to see them simultaneously. After that, single molecular manipulation has been extensively studied by different STM groups around the world, and various sorts of single molecular manipulation have been demonstrated.[72–82]

The most fascinating results of single-molecule manipulation are real-time chemical reactions realized in real space with the aid of the STM tip. Chemical reaction of two individual molecules was realized and directly visualized with STM manipulation,[83] which before could only be seen in a textbook as a formula. Moreover, it also has the capability to modify molecules by cutting chemical bonds in a controlled way.[84] However, examples of function-control *via* STM manipulation are still few, since this requires not only precise control of molecular structures but also accurate activation of different electron tunnelling processes as well as the specific chemical bonds. In our previous work, we have shown that not only the structure, but also the electronic states and magnetism of a single molecule can be manipulated in a controllable manner.[85] A single CoPc molecule adsorbed on an Au(111) surface shows a spin-degenerated nonmagnetic state due to molecule–surface interaction, in contrast to the paramagnetic state in a free CoPc molecule. We found that the magnetism can be readily recovered in such an adsorbed CoPc by sequentially dehydrogenating the four lobes of the molecule with hot electrons injected from the STM tip (Fig. 6). In these procedures hydrogen atoms are cut off the molecule by energetic electrons in analogue to surgery with knives or radiation. This work demonstrates an early example that the physical property of a molecule can be manipulated *via* a tip-induced chemical reaction, revealing the unprecedented ability of single-molecular manipulation.

3.1 Tip-induced single-molecule tautomerization

As another successive work, we further demonstrated the control of the electronic properties of single molecules by tautomerization. In chemistry, tautomerization conventionally refers to the interconverting chemical reaction that occurs between

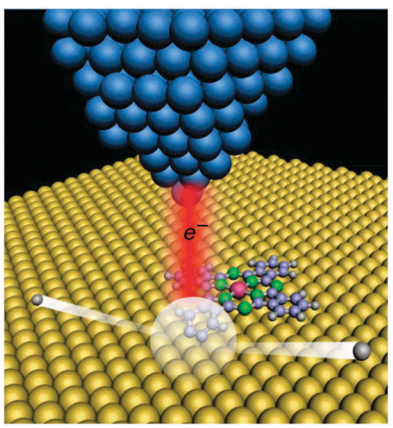

Fig. 6 Schematic drawing of STM-induced single molecule dehydrogenation. The two hydrogen atoms in one lobe of a single CoPc are dissociated by the hot electrons injected by the STM tip.

Published on 20 May 2013. Downloaded by University of Science and Technology of China on 10/07/2013 12:30:27.

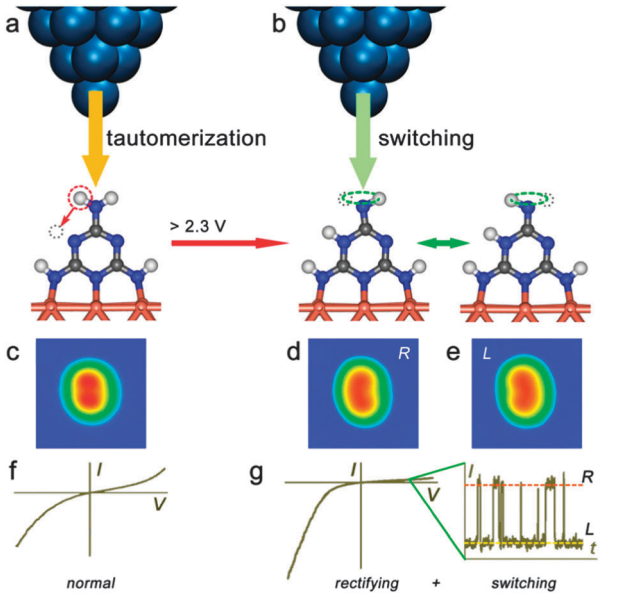

Fig. 7 Tautomerization of single chemisorbed melamine molecules. (a) Schematic of the tautomerization of a chemisorbed melamine molecule. (b) Schematic of the switching effect between the two configurations of the tautomerized molecule. (c–e) Corresponding STM images of the chemisorbed and tautomerized molecule. (f) A representative *I–V* curve showing symmetric transport behaviour of the chemisorbed molecule with symmetric structure. (g) The *I–V* curve of the tautomerized molecule showing rectifying behaviour and a typical *I–t* curve (sample bias = −0.6 V) shows that the tautomerized molecule is switching between two metastable configurations. (Modified with permission from ref. 86. Copyright 2009 National Academy of Sciences, USA.)

the constitutional isomers of organic compounds by interior transfer of a hydrogen atom or proton. We showed that single-molecule tautomerization can be realized and evidenced by an STM tip with hot tunnelling electrons.[86] Melamine, a widely used industrial material, was used as an example.

Single melamine molecules are found to be dehydrogenated and firmly bound to the Cu substrate when adsorbed on a Cu(100) surface at room temperature. The STM image shows a symmetric ''dumbbell'' shape, in accordance with the symmetry of the molecular structure (Fig. 7a and c). The transport property of the molecule in the tunnelling junction exhibits symmetric *I–V* behaviour with respect to the polarity of bias voltages in the *I–V* curve (Fig. 7f), *i.e.*, the adsorbed melamine acts as a normal conducting molecule in which electron transport is dominated by an elastic electron-tunnelling process. Interestingly, we found the transport behaviour can be greatly changed *via* STM manipulation: the molecule presents a rectifying behaviour after it is tautomerized by applying a voltage pulse (>+2.3 V). In the tautomerization a hydrogen atom is transferred from the top amino group to a neighbouring nitrogen atom in the triazine ring (Fig. 7b), as a result the STM image changes to a ''cashew nut'' pattern (Fig. 7d). This tautomerization reduces the symmetry of the molecule and its π system, resulting in the increase of molecular local DOS below the Fermi level and producing the rectification. The *I–V* curve of the tautomerized molecule shows a rectification ratio of about 20–25 at 2 V (Fig. 7g). Moreover, the tautomerized molecule turns out to be a bistable switch. The molecule can switch between two configurations that differ in the orientation of the top N–H bond as shown in Fig. 7b. This switching behaviour can also be observed in the images, where the ''cashew nut'' can change its directions under a certain bias voltages (Fig. 7d and e). The bias-dependent fluctuation features obtained in the *I–t* curves further confirm the switching behaviour (Fig. 7g). From our first-principles calculations, we may attribute the switching behaviour to the switching of an N–H bond between two configurations of the asymmetric tautomer, which is triggered by turning on inelastic multi-electron scattering processes. This instance shows the capability of STM to engineer multifunctional building blocks at the single-molecule scale by taking advantage of delicate control over individual quantum transport channels.

3.2 Tip-induced chemical reactions on catalytic surfaces

STM offers an ideal tool to control chemical reactions of individual molecules on a surface.[85–88] In the model system of the TiO_2(110)-1×1 surface for catalytic and photocatalytic studies, the understanding of the chemical reactions of O_2,[89–91] H_2O,[39,92] CO,[38,93] and CO_2[94–96] is a fundamental issue for many of the complicated reactions on this surface, which have attracted extensive study and interest for insight into the catalytic mechanism. The chemistry of O_2 on TiO_2(110)-1×1 plays an important role in the catalytic and photocatalytic processes, such as oxidation of CO and organic pollutants.[14,18,19,97,98] A fundamental question is whether the activated species is molecular O_2 or dissociative O_2. We performed a study on the adsorption behaviour of molecular O_2 at O_V and its dissociation process induced by the STM tip.[91] Fig. 8a shows the optimized structure of a singly adsorbed molecular O_2 at O_V, which has a flat-lying configuration with the O–O bond perpendicular to the O_b row. In the empty state STM image, the molecular O_2 at O_V shows a misty feature as marked by the yellow square in the lower panel of Fig. 8a. During STM scanning, the molecular O_2 becomes unstable, especially at relatively high bias voltages above 1.0 V. An intermediate state was imaged as a pair of protrusions at opposite Ti^{4+} sites, as shown in Fig. 8b. On the basis of our DFT calculations, we suggest the metastable inclined configurations of O_2 (Fig. 8b) are excited by the inelastic tunnelling electrons. By measuring the *I–t* curves at the molecular O_2, we observed that there is a switching behaviour between the inclined configuration and the flat-lying configuration of O_2 at O_V, which results in the intermediate state of paired protrusions in the STM image. Such an intermediate state should not be a dissociative O_2. However, O_2 can be finally dissociated through this intermediate state, with an O healing the O_V (O_b) and producing an O adatom (O_{ad}) at the near Ti^{4+} site (Fig. 8c). By adsorbing CO on TiO_2(110) surface with pre-adsorbed O_{ad}, it is observed that the O_{ad} does not show obvious reactivity with CO at low temperature.[93] Instead, a possible mechanism that the molecular O_2 may photo-oxidize CO through a two-step reaction sequence[99] is proposed, where the observed excited inclined intermediate state of O_2 should play a key role.

 This journal is © the Owner Societies 2013

Published on 20 May 2013. Downloaded by University of Science and Technology of China on 10/07/2013 12:30:27.

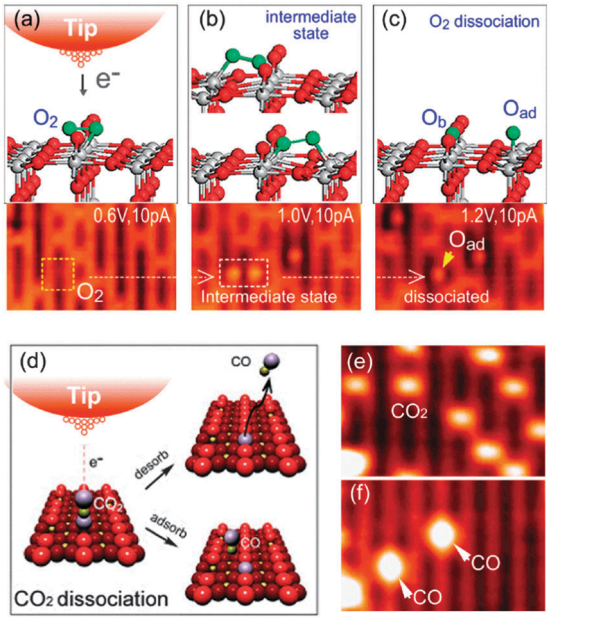

Fig. 8 Tip-induced dissociation of O_2 and CO_2 on TiO_2(110)-1×1 surface. Schematic drawings showing (a) molecular O_2 under the tip at its equilibrium flat-lying configuration, (b) molecular O_2 inclined to the left and right Ti^{4+} sites and (c) dissociated O_2. The corresponding STM images are shown at the lower panel (1.0 V, 10 pA, size: 5.2 × 3.3 nm^2). (d) Schematic drawing of the tip-induced CO_2 dissociation, leading to the healing of the O_V and either desorbed CO or adsorbed CO at Ti^{4+} site. (e) and (f) STM images of the TiO_2(110)-1×1 surface with adsorbed CO_2 at O_V before and after scanning under a high bias voltage of 2.6 V, respectively. Both images are recorded at 1.0 V, 10 pA, size: 4.9 × 3.1 nm^2. (Modified with permission from ref. 91, Copyright 2011 American Chemical Society and ref. 94, Copyright 2011 American Physical Society.)

Converting CO_2 to useful compounds through the photocatalytic reduction has been one of the most promising strategies for artificial carbon cycling.[21,100–103] The decisive step in CO_2 reduction is to effectively generate $CO_2^{\bullet -}$, which is controlled by the reduction potential of the $CO_2^{\bullet -}/CO_2$ redox couple. However, a strong energy mismatch between the reduction potential and the photo-excited electron at the conduction band occurs,[101,104,105] resulting in highly unfavourable electron transfer to the adsorbed CO_2 molecules. We find that the dissociation behaviours of CO_2 under various applied bias voltages can be used to detect the reduction potential of CO_2 at a solid interface.[94] The reduction potential was previously measured mainly at a liquid interface.[106–108] For a CO_2 molecule adsorbed at an O_V site of the TiO_2(110)-1×1 surface (Fig. 8d), it can be dissociated when a voltage pulse is applied or the surface is scanned by the STM tip with a high bias voltage, resulting in one O atom to heal the O_V and either a desorbed CO or an adsorbed CO at a Ti^{4+} site of the surface. Fig. 8e and f show the representative STM images before and after scanning under a high bias voltage of 2.6 V. It can be seen that the all of CO_2 was dissociated after 2.6 V scanning (Fig. 8f). The left-hand protrusions at the Ti^{4+} sites can be attributed to the presence of CO from the dissociation of CO_2. Such dissociation behaviour shows dependence on the applied bias voltage. A threshold bias voltage of 1.8 V is obtained, and rapid increased dissociation fractions of CO_2 occur at around 2.3 V. Theoretical calculations of the PDOS of the adsorbed CO_2 molecule at O_V show the LUMO locates above the CB onset of TiO_2 by 2.3 eV (*i.e.* 2.7 eV above the Fermi level) and strongly hybridizes with the Ti 3d orbital of the O_V. The unoccupied hybridized states are also found to spread over certain energy ranges below the LUMO. We may thus suggest that the threshold voltage is associated with the electron injection through hybridized states, while the voltage for the rapid increase of the dissociation fraction is associated with the electron injection through the LUMO. The hybridized states and the LUMO can act as the electron acceptor states. Since the STM electron tunnelling follows Fermi's golden rule, the injection of tunnelling electrons to CO_2 should be a sudden process. Once the electron is injected, the CO_2 changes from the ground state to the activated state of $CO_2^{\bullet -}$. The energy of 2.3 eV should reflect the potential for $CO_2/CO_2^{\bullet -}$ coupling under a sudden tunnelling electron excitation. This value is much smaller than the estimated value of 3.5 eV by Indrakanti *et al.*[105] and larger than the value of 1.6 eV (or −1.9 V *versus* standard hydrogen electrode (SHE)) in the aqueous solution.[106] It should be noted that if the $CO_2^{\bullet -}$ excitation is an adiabatic process, the reduction potential of $CO_2/CO_2^{\bullet -}$ couple should be lower than that of a sudden process. The dissociation rate (R_d) is measured as a function of the tunnelling current (I) at different bias voltages, following the power-law relationship $R_d \propto I^n$. In the log–log plot, the fitted data show the slope $n = 0.98 \pm 0.10$ (2.6 V), 0.96 ± 0.07 (2.4 V), and 1.05 ± 0.01 (2.2 V) respectively, indicating a single electron process in CO_2 dissociation. Our findings also imply that such a CO_2 reduction process may not happen by photo-generated electrons, since the photo-generated electrons may rapidly thermalize to the CB edge, which is much lower than the reduction potential of the $CO_2/CO_2^{\bullet -}$ couple.

The water splitting on the photocatalyst TiO_2 surface is one of the fundamental processes that has significant implications in solar energy conversion and hydrogen energy technology.[18,109–111] Previous STM studies focused on the O_V defect-assisted dissociation of H_2O molecules.[112–116] It is found the single H_2O molecule dissociated at O_V with one H transferring to a nearby bridging O site yielding a pair of OH_b groups. In this dissociation process, the O_V is healed and thus may not support sustained activity. Actually, it is observed that the H_2O molecules prefer to adsorb at the Ti^{4+} sites at a low temperature of 80 K, showing as round spots as shown in Fig. 9a. The H_2O at Ti^{4+} site is quite stable without any diffusion and dissociation at 80 K, unless a high voltage pulse is applied. As shown in Fig. 9b, when a 2.4 V pulse is applied at the lower-left H_2O molecule, it changes to a fuzzy spot at exactly the same site where the H_2O molecule originally adsorbed. Such a fuzzy spot is also identified as a hydroxyl group at Ti^{4+} (OH_t), which is produced from the tip-induced dehydrogenation of the H_2O molecule. The fuzzy OH_t can be further dissociated to an oxygen adatom (O_{ad}) (Fig. 9c). A similar dissociation can be obtained by direct removal of both hydrogens by applying a higher voltage pulse of 2.8 V (Fig. 9a and b). The processes are schematically shown in

Published on 20 May 2013. Downloaded by University of Science and Technology of China on 10/07/2013 12:30:27.

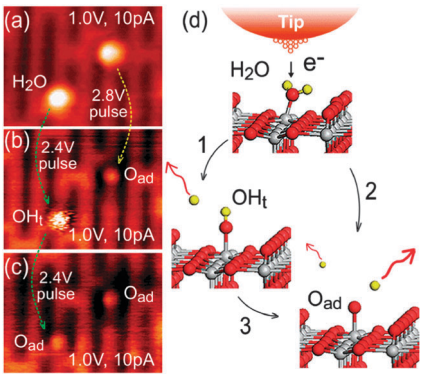

Fig. 9 Tip-induced dissociation of H_2O on a TiO_2(110)-1×1 surface. (a–c) STM images (size: 3.9 × 3.0 nm^2, imaged at 1.0 V and 10 pA, 80 K) of the tip-induced water dissociation to produce OH_t or oxygen adatom (O_{ad}) under different applied bias voltages. (d) Schematic drawings showing structural models of different processes of the tip-induced water dissociation. (Reprinted with permission from ref. 39. Copyright 2012 American Chemical Society.)

Fig. 9d. Such processes partly mimic the reduction of adsorbed water molecules through attachment of electrons injected by the STM tip, which shows quite different behaviour from the photocatalytic dissociation of H_2O under UV irradiation (see below in Section 4.1).

4. Extended STM functions on photochemistry and electroluminescence

The functions of STM can be extended by combination with certain other techniques, keeping the advantage of superior stability and high resolution in real space. Here we show two examples in photochemistry and electroluminescence at the single-molecule level.

4.1 *In situ* characterization of photocatalytic reactions of single molecules

Because of its potential applications in solar energy conversion and clean hydrogen energy technology,[15–20,111] photocatalytic water splitting on TiO_2 has been intensively studied since its discovery.[117] However, it remains unclear what is the actual initial step for the water splitting reaction and it is also argued whether the adsorbed H_2O molecules at Ti^{4+} sites could be oxidized by the photogenerated holes in the valence band (Fig. 10a).[19,118–121] Salvador suggested that the water species specifically adsorbed on terminal Ti atoms could not be photo-oxidized since the photogenerated VB holes did not have enough potential.[111,118] Nakamura and Nakato suggested that the water photooxidation should be initiated by nucleophilic attack of an H_2O molecule on a photogenerated hole at a surface lattice O site, not by oxidation of surface OH group by the hole.[119,120] However, Valdés *et al.* suggested that the photogenerated VB holes could provide enough overpotential for water photooxidation through one-electron transfer steps on the basis of their theoretical calculations.[121] By using the *in situ* photochemical STM method, we provide direct evidence that the initial step of the water splitting reaction can be photocatalytic for the H_2O molecules at terminal Ti^{4+} sites on the TiO_2(110)-1×1 surface.[39] By comparing the images before and after UV illumination, one can directly see the changes induced by adsorbed H_2O molecules (Fig. 10b and c). In the experiment, the ultra-violet (UV) light was shone on the surface area under the STM tip. To avoid the shadowing effect[112] of the tip, the tip was traced back by about 10 μm during UV illumination. After 400 nm light illumination for 1 hour, the dissociation of individual H_2O molecules at terminal Ti^{4+} sites was directly observed. The photocatalyic dissociation of H_2O produces an OH_b group at the nearest bridging oxygen (O_b) sites due to the H transfer and an OH_t (Fig. 10b and c). The OH_t species may occur at a Ti^{4+} site away from the original position by several lattice distances, or it may desorb from the surface. The observed H_2O dissociation under UV illumination is schematically illustrated in Fig. 10d_1–d_4: one of the H atoms transfers to the opposite O_b site forming an OH_b and the left OH either desorbs from surface as an •OH radical (Fig. 10d_3) or adsorbs at a near Ti^{4+} as an OH_t (Fig. 10d_4). It is found that the H_2O can be dissociated only under light illumination with a wavelength shorter than 400 nm, which corresponds to the TiO_2 bandgap of 3.05 eV. That is, the H_2O dissociation should be a

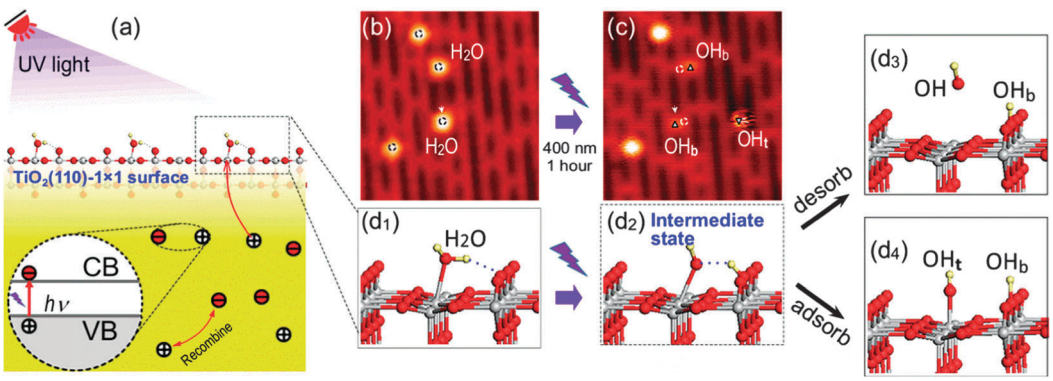

Fig. 10 Photocatalytic splitting of H_2O on terminal Ti^{4+} sites. (a) Schematic drawings of the photogenerated electron–hole pair by bandgap excitation and hole transfer to adsorbed H_2O molecules. (b) STM image of the H_2O adsorbed TiO_2(110)-1×1 surface. (c) The same area after 1 hour 400 nm light irradiation. Image condition: 1.0 V and 10 pA, 80 K, size: 6.3 × 6.6 nm^2. (d_1–d_4) Structure models of photocatalytic H_2O dissociation at a Ti^{4+} site. (Modified with permission from ref. 39. Copyright 2012 American Chemical Society.)

 This journal is © the Owner Societies 2013

Published on 20 May 2013. Downloaded by University of Science and Technology of China on 10/07/2013 12:30:27.

photocatalytic process. This process is obviously different from the process with the electrons injected by the STM tip shown above (Fig. 9). Such a difference also suggests the photocatalytic H_2O dissociation is an oxidation process by photogenerated holes in valence band (Fig. 10a). Similar photocatalytic dissociation of methanol molecules on the TiO_2(110)-1×1 surface is also observed in our STM studies along with the time-dependent two-photon photoemission (TD-2PPE) method.[122] We suggest these two molecules should undergo a similar dissociation mechanism. Petek and Zhao discussed the hole mediated processes in methanol dissociation.[123] We refer to that paper for detailed theoretical analysis. In comparison with water, methanol shows a quite high dissociation efficiency under UV illumination, which may be attributed to its nature as a hole scavenger in photocatalytic reactions.[124–127]

4.2 Tip-induced electroluminescence at the single-molecule level

Light emission is an important general phenomenon of matter in physical sciences and technologies and leads to various applications that are of benefit to human civilization. To excite light emission at the single-molecule level in a controlled manner has been pursued for years because it is of particular importance for the understanding of energy transfer and light manipulation at the nanoscale and for the development of nanoscale optoelectronic integration.[128,129] Photon emission in STM was firstly reported from Ta and Si(111) by Gimzewski *et al.* in 1988.[130] After that, extensive research on STM-induced luminescence (STML) has been reported on metal surfaces,[131,132] semiconductors[133,134] and molecules.[135–141] These studies suggested that the local plasmon modes defined by the metallic tip and surface play a very important role in the generation of molecular fluorescence.

In principle, molecular fluorescence should be controlled over a wide energy range and with a selected frequency by tuning the emission from various vibronic transitions through resonance enhancement near plasmonic substances. However, early reports suggest the optical excitations of polyatomic molecules near metals follow Kasha's rule with radiative decay from the lowest excited state only.[142–146] It was a challenging issue to generate hot luminescence from highly excited vibronic states in molecules near metals. The key problem is whether one can create a situation in which the radiative decay directly from higher vibronic levels in the excited state can become comparable to rapid internal relaxation in the excited state.[147] STM provides a unique route to achieve such a situation owing to the strong near-field enhancement of resonant plasmons that are highly confined inside a nanocavity defined by the STM tip and the metal substrate. In such a system, the spectral profile of the nanocavity plasmons (NCPs) and the NCP resonance mode can be readily tuned by modifying the tip conditions.

We have demonstrated that by taking the advantage of the STM nanocavity, resonance hot electroluminescence arising directly from higher vibronic levels of the singlet excited state for porphyrin molecules confined inside the nanocavity was realized by tuning spectrally the frequency of the plasmons.[141] We also revealed the generation of unexpected upconversion electroluminescence with the energy of emitted photons that is higher than that of excitation electrons.[141] In this work, samples of multilayer tetraphenyl porphyrin (TPP) adsorbed on metal surfaces were used for their well-defined double-peak *Q*-band emission. The top layer of TPP molecules act as a light emitter while the underlying layers act as decoupling layer to avoid fluorescence quenching. Fig. 11 shows the schematic of the experiments, the molecular structure and the STM image of a sample of five-monolayer TPP. All STML spectra show clearly the molecular-specific double-peak features with peaks located at ~1.89 eV and ~1.73 eV, which have been attributed to the (0, 0) and (0, 1) electronic transitions respectively (tip 3 in Fig. 11c). Surprisingly, the spectral profile can be remarkably modified with different tips depending on the tip status and consequent NCP resonance mode as shown in Fig. 11c. The local plasmon resonance mode of the nanocavity can be spectrally tuned to match a particular (ν', ν) radiative transition of the TPP molecules and greatly enhance the corresponding vibronic transition (lightly shaded peak in Fig. 11c). The unprecedented occurrence of a low-energy (0, 2) band around 1.6 eV and a high-energy (1, 0) and (2, 0) hot luminescence band around 2.05 eV and 2.2 eV, respectively, were evidenced simultaneously with the conventional two *Q*-band emissions (0, 0) and (0, 1). The mechanism of the hot luminescence is illustrated in Fig. 11d. This is the first solid observation of the tuning the ''colour'' (frequency) of molecular resonance over a wide spectra range. Moreover, we even observed an intense (1, 0) band at excitation voltages lower than the optical bandgap of the TPP molecules. The onset voltage for molecular electroluminescence is around +1.6 V. That is to say, the emission of ''energy-forbidden'' upconversion photons for which the energy $h\nu$ exceeds the energy of a tunnelling electron is allowed in such a nanocavity. Unlike the linear relation at a bias larger than the optical bandgap (for example, +2.5 V) that suggests essentially single-step excitation events, the current dependency of photon intensities at +1.8 V in the ''energy-forbidden'' regime reveals a nonlinear behaviour with a power-law exponent of ~1.6. This nonlinear behaviour indicates the possibility of involvement of a two or multi-step excitation processes for the upconversion electroluminescence to satisfy the energy conservation. These observations demonstrate that the STM can provide a nanocavity with local plasmons behaving like an energy-tunable strong coherent light source. The generation of broadband molecular fluorescence by resonant nanocavity plasmons emphasizes the importance of plasmon-exciton coupling in the nano-environment and sheds new light on molecule-based nanophotonics and nanoplasmonics, which is of great scientific and technological importance for various applications.

5. Summary and perspective

In summary, we review our recent progress on STM investigation at the single-molecule level. It is worth to note the instances introduced in this Perspective only show limited

Published on 20 May 2013. Downloaded by University of Science and Technology of China on 10/07/2013 12:30:27.

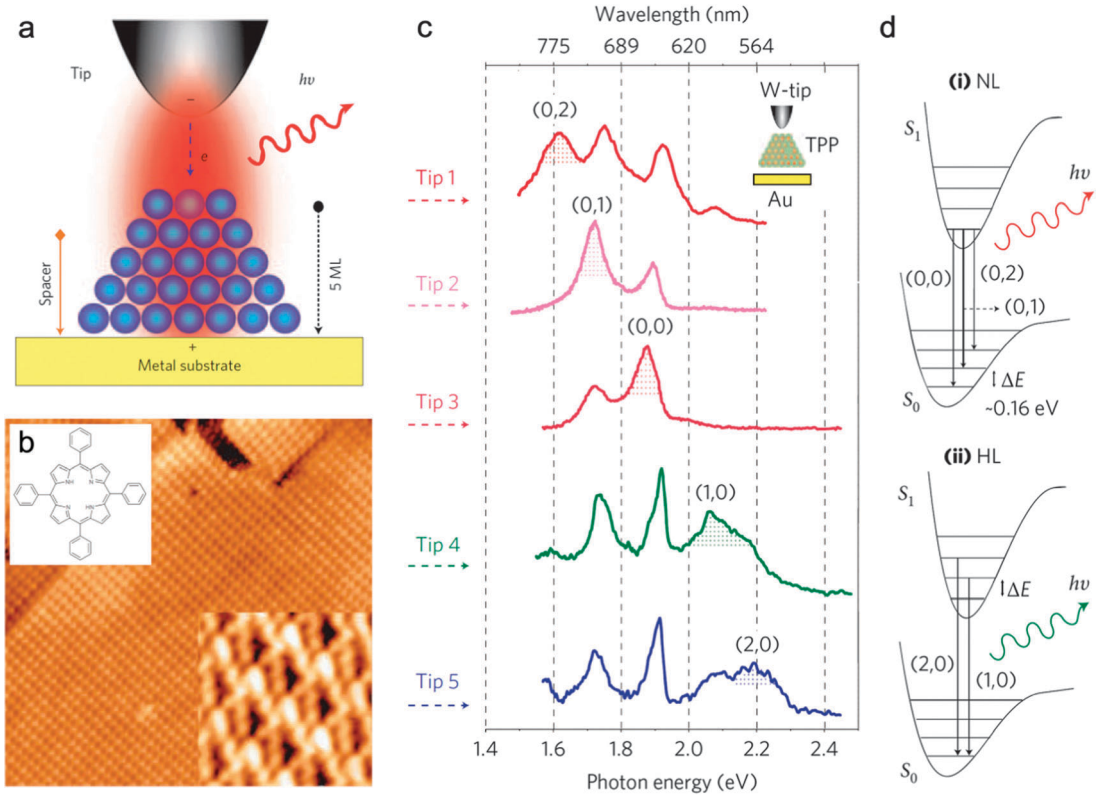

Fig. 11 Tunable molecular electroluminescence by resonant NCP in local STM cavities. (a) Schematic junction geometry with multi-monolayer stacking and localized electrical excitation from a nanotip. (b) The molecular structure of TPP and the STM image showing highly ordered molecular stacking for 5-ML TPP molecules on Au(111) (55 × 55 nm^2, +2.5 V, 2 pA). The right inset is a high-resolution image with each molecule resolved into one bright lobe and several other relatively dark lobes (6 × 6 nm^2, +2.5 V, 2 pA). (c) STML spectra acquired from the sample using different tips with particular tip status, showing great resonance enhancement of the particular emission peak (lightly shaded) and pronounced spectral profile modifications. The peak assignment was based on the equispacing feature of vibrational levels. (d) Schematic of various vibronic transitions: (i) normal luminescence (NL) emitting from $S_1(0)$ and (ii) hot luminescence (HL) from highly excited $S_1(1)$ or $S_1(2)$. All spectra were acquired at +2.5 V and 200 pA. (Modified with permission from ref. 141. Copyright 2010 Nature Publishing Group.)

advantages of what one can get from the powerful tool of STM. To fulfil the desire to develop future nano- and quantum-devices, one needs to investigate the quantum phenomena at the single-molecule level, as single molecules are such a unique candidate for quantum design owing to their identity and flexibility in structure, and the quantum-mechanical nature of their physical properties. More efforts are always ongoing to explore new applications and to extend the capability of STM by combining STM with other techniques. A promising implementation is to combine STM/AFM with electron-spin resonance techniques,[148,149] which will push the spatial limit of manipulating the quantum levels with microwaves to individual molecules. Once the technique is developed, it will greatly promote the implementation of solid-state quantum information, besides other scenarios like the colour centre in diamond and dopants in silicon, because the molecules are much easier to manipulate in both energy space and real space. Another promising technique is to combine STM with Raman spectroscopy, an extremely useful technique for chemical identification of a macro-amount of molecules. The combination of STM with Raman spectroscopy on single molecules is now becoming very close to reality thanks to the nature of so-called tip-enhanced Raman spectroscopy developed recently.[150]

We expect more joint techniques to emerge in the near future by taking the unique advantages of the STM tip, providing more powerful tools for the growing requirements of new materials design and for understanding the mechanisms of chemical reactions at the molecular scale.

Acknowledgements

This work is supported by the National Basic Research Program of China (Grant No. 2011CB921400), by the National Natural Science Foundation of China and by Chinese Academy of Sciences.

References

1 G. Binnig, H. Rohrer, C. Gerber and E. Weibel, *Phys. Rev. Lett.*, 1982, **49**, 57–61.
2 G. Binnig, H. Rohrer, C. Gerber and E. Weibel, *Appl. Phys. Lett.*, 1982, **40**, 178–180.
3 J. P. Rabe and S. Buchholz, *Science*, 1991, **253**, 424–427.
4 C. A. Widrig, C. A. Alves and M. D. Porter, *J. Am. Chem. Soc.*, 1991, **113**, 2805–2810.

 This journal is © the Owner Societies 2013

Published on 20 May 2013. Downloaded by University of Science and Technology of China on 10/07/2013 12:30:27.

5 Q. H. Wang and M. C. Hersam, *Nat. Chem.*, 2009, **1**, 206–211.
6 J. G. Hou, J. L. Yang, H. Q. Wang, Q. X. Li, C. G. Zeng, L. F. Yuan, B. Wang, D. M. Chen and Q. S. Zhu, *Nature*, 2001, **409**, 304–305.
7 T. A. Jung, R. R. Schlittler and J. K. Gimzewski, *Nature*, 1997, **386**, 696–698.
8 G. P. Lopinski, D. J. Moffatt, D. D. M. Wayner and R. A. Wolkow, *Nature*, 1998, **392**, 909–911.
9 J. G. Hou, J. L. Yang, H. Q. Wang, Q. X. Li, C. G. Zeng, H. Lin, B. Wang, D. M. Chen and Q. S. Zhu, *Phys. Rev. Lett.*, 1999, **83**, 3001–3004.
10 N. J. Tao, *Nat. Nanotechnol.*, 2006, **1**, 173–181.
11 B. C. Stipe, M. A. Rezaei and W. Ho, *Science*, 1998, **280**, 1732–1735.
12 B. C. Stipe, M. A. Rezaei and W. Ho, *Phys. Rev. Lett.*, 1998, **81**, 1263–1266.
13 A. L. Linsebigler, G. Q. Lu and J. T. Yates, *Chem. Rev.*, 1995, **95**, 735–758.
14 T. L. Thompson and J. T. Yates, *Chem. Rev.*, 2006, **106**, 4428–4453.
15 C. L. Pang, R. Lindsay and G. Thornton, *Chem. Soc. Rev.*, 2008, **37**, 2328–2353.
16 Z. Dohnálek, I. Lyubinetsky and R. Rousseau, *Prog. Surf. Sci.*, 2010, **85**, 161–205.
17 U. Diebold, *Surf. Sci. Rep.*, 2003, **48**, 53–229.
18 A. Fujishima, X. T. Zhang and D. A. Tryk, *Surf. Sci. Rep.*, 2008, **63**, 515–582.
19 M. A. Henderson, *Surf. Sci. Rep.*, 2011, **66**, 185–297.
20 A. Kudo and Y. Miseki, *Chem. Soc. Rev.*, 2009, **38**, 253–278.
21 M. Gratzel, *Nature*, 2001, **414**, 338–344.
22 S. Wendt, R. Schaub, J. Matthiesen, E. K. Vestergaard, E. Wahlström, M. D. Rasmussen, P. Thostrup, L. M. Molina, E. Lægsgaard, I. Stensgaard, B. Hammer and F. Besenbacher, *Surf. Sci.*, 2005, **598**, 226–245.
23 G. H. Enevoldsen, A. S. Foster, M. C. Christensen, J. V. Lauritsen and F. Besenbacher, *Phys. Rev. B: Condens. Matter Mater. Phys.*, 2007, **76**, 205415.
24 X. F. Cui, Z. Wang, S. J. Tan, B. Wang, J. L. Yang and J. G. Hou, *J. Phys. Chem. C*, 2009, **113**, 13204–13208.
25 S. Suzuki, K.-i. Fukui, H. Onishi and Y. Iwasawa, *Phys. Rev. Lett.*, 2000, **84**, 2156–2159.
26 N. A. Deskins, R. Rousseau and M. Dupuis, *J. Phys. Chem. C*, 2009, **113**, 14583–14586.
27 C. Di Valentin, G. Pacchioni and A. Selloni, *Phys. Rev. Lett.*, 2006, **97**, 166803.
28 K. Mitsuhara, H. Okumura, A. Visikovskiy, M. Takizawa and Y. Kido, *J. Chem. Phys.*, 2012, **136**, 124707.
29 Z. Zhang, K. Cao and J. T. Yates, *J. Phys. Chem. Lett.*, 2013, **4**, 674–679.
30 A. C. Papageorgiou, N. S. Beglitis, C. L. Pang, G. Teobaldi, G. Cabailh, Q. Chen, A. J. Fisher, W. A. Hofer and G. Thornton, *Proc. Natl. Acad. Sci. U. S. A.*, 2010, **107**, 2391–2396.
31 M. Batzill, K. Katsiev, D. J. Gaspar and U. Diebold, *Phys. Rev. B: Condens. Matter Mater. Phys.*, 2002, **66**, 235401.
32 Z. Zhang, O. Bondarchuk, B. D. Kay, J. M. White and Z. Dohnálek, *J. Phys. Chem. B*, 2006, **110**, 21840–21845.
33 N. A. Deskins, R. Rousseau and M. Dupuis, *J. Phys. Chem. C*, 2010, **114**, 5891–5897.
34 C. Di Valentin, G. Pacchioni and A. Selloni, *J. Phys. Chem. C*, 2009, **113**, 20543–20552.
35 V. E. Henrich, G. Dresselhaus and H. J. Zeiger, *Phys. Rev. Lett.*, 1976, **36**, 1335–1339.
36 M. A. Henderson, W. S. Epling, C. H. F. Peden and C. L. Perkins, *J. Phys. Chem. B*, 2003, **107**, 534–545.
37 T. Minato, Y. Sainoo, Y. Kim, H. S. Kato, K. Aika, M. Kawai, J. Zhao, H. Petek, T. Huang, W. He, B. Wang, Z. Wang, Y. Zhao, J. L. Yang and J. G. Hou, *J. Chem. Phys.*, 2009, **130**, 124502.
38 Y. Zhao, Z. Wang, X. F. Cui, T. Huang, B. Wang, Y. Luo, J. L. Yang and J. G. Hou, *J. Am. Chem. Soc.*, 2009, **131**, 7958–7959.
39 S. J. Tan, H. Feng, Y. F. Ji, Y. Wang, J. Zhao, A. D. Zhao, B. Wang, Y. Luo, J. L. Yang and J. G. Hou, *J. Am. Chem. Soc.*, 2012, **134**, 9978–9985.
40 C. J. Chen, *Introduction to Scanning Tunneling Microscopy*, Oxford University Press, New York, 1993.
41 E. J. Heller, M. F. Crommie, C. P. Lutz and D. M. Eigler, *Nature*, 1994, **369**, 464–466.
42 S. H. Pan, E. W. Hudson, K. M. Lang, H. Eisaki, S. Uchida and J. C. Davis, *Nature*, 2000, **403**, 746–750.
43 X. H. Lu, M. Grobis, K. H. Khoo, S. G. Louie and M. F. Crommie, *Phys. Rev. Lett.*, 2003, **90**, 096802.
44 K. D. Wang, J. Zhao, S. F. Yang, L. Chen, Q. X. Li, B. Wang, S. H. Yang, J. L. Yang, J. G. Hou and Q. S. Zhu, *Phys. Rev. Lett.*, 2003, **91**, 185504.
45 J. Repp, G. Meyer, S. M. Stojković, A. Gourdon and C. Joachim, *Phys. Rev. Lett.*, 2005, **94**, 026803.
46 M. Grobis, K. H. Khoo, R. Yamachika, X. H. Lu, K. Nagaoka, S. G. Louie, M. F. Crommie, H. Kato and H. Shinohara, *Phys. Rev. Lett.*, 2005, **94**, 136802.
47 T. Huang, J. Zhao, M. Feng, A. A. Popov, S. Yang, L. Dunsch and H. Petek, *Nano Lett.*, 2011, **11**, 5327–5332.
48 K. Muthukumar, A. Stróżecka, J. Mysliveček, A. Dybek, T. J. S. Dennis, B. Voigtländer and J. A. Larsson, *J. Phys. Chem. C*, 2013, **117**, 1656–1662.
49 J. H. Warner, A. A. R. Watt, L. Ge, K. Porfyrakis, T. Akachi, H. Okimoto, Y. Ito, A. Ardavan, B. Montanari, J. H. Jefferson, N. M. Harrison, H. Shinohara and G. A. D. Briggs, *Nano Lett.*, 2008, **8**, 1005–1010.
50 C. S. Allen, Y. Ito, A. W. Robertson, H. Shinohara and J. H. Warner, *ACS Nano*, 2011, **5**, 10084–10089.
51 Y. Sato, K. Suenaga, S. Okubo, T. Okazaki and S. Iijima, *Nano Lett.*, 2007, **7**, 3704–3708.
52 A. L. Vázquez de Parga, O. S. Hernán, R. Miranda, A. L. Yeyati, N. Mingo, A. Martín-Rodero and F. Flores, *Phys. Rev. Lett.*, 1998, **80**, 357–360.
53 J. R. Hahn, H. J. Lee and W. Ho, *Phys. Rev. Lett.*, 2000, **85**, 1914–1917.
54 B. Li, H. Q. Wang, J. L. Yang and J. G. Hou, *Ultramicroscopy*, 2004, **98**, 317–334.

Published on 20 May 2013. Downloaded by University of Science and Technology of China on 10/07/2013 12:30:27.

55 L. Bartels, G. Meyer and K. H. Rieder, *Appl. Phys. Lett.*, 1997, **71**, 213–215.
56 Z. T. Deng, H. Lin, W. Ji, L. Gao, X. Lin, Z. H. Cheng, X. B. He, J. L. Lu, D. X. Shi, W. A. Hofer and H. J. Gao, *Phys. Rev. Lett.*, 2006, **96**, 156102.
57 A. N. Chaika, V. N. Semenov, S. S. Nazin, S. I. Bozhko, S. Murphy, K. Radican and I. V. Shvets, *Phys. Rev. Lett.*, 2007, **98**, 206101.
58 M. Bode, *Rep. Prog. Phys.*, 2003, **66**, 523–582.
59 J. R. Hahn and W. Ho, *Phys. Rev. Lett.*, 2001, **87**, 196102.
60 T. Ohshiro, T. Ito, P. Bühlmann and Y. Umezawa, *Anal. Chem.*, 2001, **73**, 878–883.
61 C. Weiss, C. Wagner, C. Kleimann, M. Rohlfing, F. S. Tautz and R. Temirov, *Phys. Rev. Lett.*, 2010, **105**, 086103.
62 Z. Y. Li, B. Li, J. L. Yang and J. G. Hou, *Acc. Chem. Res.*, 2010, **43**, 954–962.
63 Z. P. Hu, L. Chen, A. D. Zhao, Z. Y. Li, B. Wang, J. L. Yang and J. G. Hou, *J. Phys. Chem. C*, 2008, **112**, 15603–15606.
64 L. Chen, Z. P. Hu, A. D. Zhao, B. Wang, Y. Luo, J. L. Yang and J. G. Hou, *Phys. Rev. Lett.*, 2007, **99**, 146803.
65 C. G. Zeng, H. Q. Wang, B. Wang, J. L. Yang and J. G. Hou, *Appl. Phys. Lett.*, 2000, **77**, 3595–3597.
66 N. P. Guisinger, M. E. Greene, R. Basu, A. S. Baluch and M. C. Hersam, *Nano Lett.*, 2004, **4**, 55–59.
67 N. P. Guisinger, N. L. Yoder and M. C. Hersam, *Proc. Natl. Acad. Sci. U. S. A.*, 2005, **102**, 8838–8843.
68 A.-S. Hallbäck, B. Poelsema and H. J. W. Zandvliet, *Appl. Surf. Sci.*, 2007, **253**, 4066–4071.
69 T. Rakshit, G.-C. Liang, A. W. Ghosh and S. Datta, *Nano Lett.*, 2004, **4**, 1803–1807.
70 W. H. Wang, Y. F. Ji, H. Zhang, A. D. Zhao, B. Wang, J. L. Yang and J. G. Hou, *ACS Nano*, 2012, **6**, 7066–7076.
71 J. S. Foster and J. E. Frommer, *Nature*, 1988, **333**, 542–545.
72 T. A. Jung, R. R. Schlittler, J. K. Gimzewski, H. Tang and C. Joachim, *Science*, 1996, **271**, 181–184.
73 T. Komeda, Y. Kim, M. Kawai, B. N. J. Persson and H. Ueba, *Science*, 2002, **295**, 2055–2058.
74 P. Liljeroth, J. Repp and G. Meyer, *Science*, 2007, **317**, 1203–1206.
75 F. Moresco, G. Meyer, K. H. Rieder, H. Tang, A. Gourdon and C. Joachim, *Phys. Rev. Lett.*, 2001, **87**, 088302.
76 F. Moresco, G. Meyer, K. H. Rieder, H. Tang, A. Gourdon and C. Joachim, *Phys. Rev. Lett.*, 2001, **86**, 672–675.
77 G. V. Nazin, X. H. Qiu and W. Ho, *Science*, 2003, **302**, 77–81.
78 J. I. Pascual, N. Lorente, Z. Song, H. Conrad and H. P. Rust, *Nature*, 2003, **423**, 525–528.
79 J. Repp, G. Meyer, S. Paavilainen, F. E. Olsson and M. Persson, *Science*, 2006, **312**, 1196–1199.
80 J. A. Stroscio and D. M. Eigler, *Science*, 1991, **254**, 1319–1326.
81 R. Yamachika, M. Grobis, A. Wachowiak and M. F. Crommie, *Science*, 2004, **304**, 281–284.
82 J. G. Hou and A. D. Zhao, *Nano*, 2006, **1**, 15–33.
83 S. W. Hla, L. Bartels, G. Meyer and K. H. Rieder, *Phys. Rev. Lett.*, 2000, **85**, 2777–2780.
84 W. Ho, *J. Chem. Phys.*, 2002, **117**, 11033–11061.
85 A. D. Zhao, Q. X. Li, L. Chen, H. J. Xiang, W. H. Wang, S. Pan, B. Wang, X. D. Xiao, J. L. Yang, J. G. Hou and Q. S. Zhu, *Science*, 2005, **309**, 1542–1544.
86 S. Pan, Q. Fu, T. Huang, A. D. Zhao, B. Wang, Y. Luo, J. L. Yang and J. G. Hou, *Proc. Natl. Acad. Sci. U. S. A.*, 2009, **106**, 15259–15263.
87 W. Ho, *Acc. Chem. Res.*, 1998, **31**, 567–573.
88 Y. Jiang, Q. Huan, L. Fabris, G. C. Bazan and W. Ho, *Nat. Chem.*, 2012, **5**, 36–41.
89 P. Scheiber, A. Riss, M. Schmid, P. Varga and U. Diebold, *Phys. Rev. Lett.*, 2010, **105**, 216101.
90 Z.-T. Wang, Y. Du, Z. Dohnálek and I. Lyubinetsky, *J. Phys. Chem. Lett.*, 2010, **1**, 3524–3529.
91 S. J. Tan, Y. F. Ji, Y. Zhao, A. D. Zhao, B. Wang, J. L. Yang and J. G. Hou, *J. Am. Chem. Soc.*, 2011, **133**, 2002–2009.
92 J. Lee, D. C. Sorescu, X. Y. Deng and K. D. Jordan, *J. Phys. Chem. Lett.*, 2013, **4**, 53–57.
93 Z. Wang, Y. Zhao, X. F. Cui, S. J. Tan, A. D. Zhao, B. Wang, J. L. Yang and J. G. Hou, *J. Phys. Chem. C*, 2010, **114**, 18222–18227.
94 S. J. Tan, Y. Zhao, J. Zhao, Z. Wang, C. X. Ma, A. D. Zhao, B. Wang, Y. Luo, J. L. Yang and J. G. Hou, *Phys. Rev. B: Condens. Matter Mater. Phys.*, 2011, **84**, 155418.
95 J. Lee, D. C. Sorescu and X. Y. Deng, *J. Am. Chem. Soc.*, 2011, **133**, 10066–10069.
96 D. P. Acharya, N. Camillone and P. Sutter, *J. Phys. Chem. C*, 2011, **115**, 12095–12105.
97 M. Haruta, T. Kobayashi, H. Sano and N. Yamada, *Chem. Lett.*, 1987, 405–408.
98 G. Q. Lu, A. Linsebigler and J. T. Yates, *J. Chem. Phys.*, 1995, **102**, 4657–4662.
99 Y. F. Ji, B. Wang and Y. Luo, *J. Phys. Chem. C*, 2013, **117**, 956–961.
100 H. Arakawa, M. Aresta, J. N. Armor, M. A. Barteau, E. J. Beckman, A. T. Bell, J. E. Bercaw, C. Creutz, E. Dinjus, D. A. Dixon, K. Domen, D. L. DuBois, J. Eckert, E. Fujita, D. H. Gibson, W. A. Goddard, D. W. Goodman, J. Keller, G. J. Kubas, H. H. Kung, J. E. Lyons, L. E. Manzer, T. J. Marks, K. Morokuma, K. M. Nicholas, R. Periana, L. Que, J. Rostrup-Nielson, W. M. H. Sachtler, L. D. Schmidt, A. Sen, G. A. Somorjai, P. C. Stair, B. R. Stults and W. Tumas, *Chem. Rev.*, 2001, **101**, 953–996.
101 S. C. Roy, O. K. Varghese, M. Paulose and C. A. Grimes, *ACS Nano*, 2010, **4**, 1259–1278.
102 N. S. Lewis and D. G. Nocera, *Proc. Natl. Acad. Sci. U. S. A.*, 2006, **103**, 15729–15735.
103 T. Inoue, A. Fujishima, S. Konishi and K. Honda, *Nature*, 1979, **277**, 637–638.
104 H. J. Freund and M. W. Roberts, *Surf. Sci. Rep.*, 1996, **25**, 225–273.
105 V. P. Indrakanti, J. D. Kubicki and H. H. Schobert, *Energy Environ. Sci.*, 2009, **2**, 745–758.
106 W. H. Koppenol and J. D. Rush, *J. Phys. Chem.*, 1987, **91**, 4429–4430.
107 E. Fujita, *Coord. Chem. Rev.*, 1999, **185–186**, 373–384.
108 J. Rasko and F. Solymosi, *J. Phys. Chem.*, 1994, **98**, 7147–7152.

 This journal is © the Owner Societies 2013

Published on 20 May 2013. Downloaded by University of Science and Technology of China on 10/07/2013 12:30:27.

109 B. Hammer, S. Wendt and F. Besenbacher, *Top. Catal.*, 2010, **53**, 423–430.
110 N. S. Lewis, *Nature*, 2001, **414**, 589–590.
111 P. Salvador, *Prog. Surf. Sci.*, 2011, **86**, 41–58.
112 S. C. Li, Z. Zhang, D. Sheppard, B. D. Kay, J. M. White, Y. Du, I. Lyubinetsky, G. Henkelman and Z. Dohnálek, *J. Am. Chem. Soc.*, 2008, **130**, 9080–9088.
113 S. Wendt, J. Matthiesen, R. Schaub, E. K. Vestergaard, E. Laegsgaard, F. Besenbacher and B. Hammer, *Phys. Rev. Lett.*, 2006, **96**, 066107.
114 O. Bikondoa, C. L. Pang, R. Ithnin, C. A. Muryn, H. Onishi and G. Thornton, *Nat. Mater.*, 2006, **5**, 189–192.
115 I. M. Brookes, C. A. Muryn and G. Thornton, *Phys. Rev. Lett.*, 2001, **87**, 266103.
116 Z. Zhang, O. Bondarchuk, B. D. Kay, J. M. White and Z. Dohnálek, *J. Phys. Chem. B*, 2006, **110**, 21840–21845.
117 A. Fujishima and K. Honda, *Nature*, 1972, **238**, 37–38.
118 P. Salvador, *J. Phys. Chem. C*, 2007, **111**, 17038–17043.
119 R. Nakamura and Y. Nakato, *J. Am. Chem. Soc.*, 2004, **126**, 1290–1298.
120 A. Imanishi, T. Okamura, N. Ohashi, R. Nakamura and Y. Nakato, *J. Am. Chem. Soc.*, 2007, **129**, 11569–11578.
121 Á. Valdés, Z. W. Qu, G. J. Kroes, J. Rossmeisl and J. K. Nørskov, *J. Phys. Chem. C*, 2008, **112**, 9872–9879.
122 C. Y. Zhou, Z. F. Ren, S. J. Tan, Z. B. Ma, X. C. Mao, D. X. Dai, H. J. Fan, X. M. Yang, J. LaRue, R. Cooper, A. M. Wodtke, Z. Wang, Z. Y. Li, B. Wang, J. L. Yang and J. G. Hou, *Chem. Sci.*, 2010, **1**, 575–580.
123 H. Petek and J. Zhao, *Chem. Rev.*, 2010, **110**, 7082–7099.
124 T. L. Thompson and J. T. Yates, *J. Phys. Chem. B*, 2005, **109**, 18230–18236.
125 M. M. Shen and M. A. Henderson, *J. Phys. Chem. Lett.*, 2011, **2**, 2707–2710.
126 J. Zhao, J. L. Yang and H. Petek, *Phys. Rev. B: Condens. Matter Mater. Phys.*, 2009, **80**, 235416.
127 M. A. Henderson, S. Otero-Tapia and M. E. Castro, *Faraday Discuss.*, 1999, **114**, 313–329.
128 R. R. Chance, A. Prock and R. Silbey, in *Advances in Chemical Physics*, ed. I. Prigogine and S. A. Rice, John Wiley & Sons, Inc., 2007, pp. 1–65.
129 J. J. Greffet, *Science*, 2005, **308**, 1561–1563.
130 J. K. Gimzewski, B. Reihl, J. H. Coombs and R. R. Schlittler, *Z. Phys. B: Condens. Matter*, 1988, **72**, 497–501.
131 R. Berndt, J. K. Gimzewski and P. Johansson, *Phys. Rev. Lett.*, 1991, **67**, 3796–3799.
132 G. Hoffmann, T. Maroutian and R. Berndt, *Phys. Rev. Lett.*, 2004, **93**, 076102.
133 D. L. Abraham, A. Veider, C. Schönenberger, H. P. Meier, D. J. Arent and S. F. Alvarado, *Appl. Phys. Lett.*, 1990, **56**, 1564–1566.
134 T. Tsuruoka, Y. Ohizumi, S. Ushioda, Y. Ohno and H. Ohno, *Appl. Phys. Lett.*, 1998, **73**, 1544–1546.
135 R. Berndt, R. Gaisch, J. K. Gimzewski, B. Reihl, R. R. Schlittler, W. D. Schneider and M. Tschudy, *Science*, 1993, **262**, 1425–1427.
136 G. Hoffmann, L. Libioulle and R. Berndt, *Phys. Rev. B: Condens. Matter*, 2002, **65**, 212107.
137 E. Ćavar, M. C. Blüm, M. Pivetta, F. Patthey, M. Chergui and W. D. Schneider, *Phys. Rev. Lett.*, 2005, **95**, 196102.
138 Z. C. Dong, X. L. Guo, A. S. Trifonov, P. S. Dorozhkin, K. Miki, K. Kimura, S. Yokoyama and S. Mashiko, *Phys. Rev. Lett.*, 2004, **92**, 086801.
139 H. W. Liu, Y. Le, T. Yoshinobu, Y. Aso, H. Iwasaki and R. Nishitani, *Appl. Phys. Lett.*, 2006, **88**, 061901.
140 X. H. Qiu, G. V. Nazin and W. Ho, *Science*, 2003, **299**, 542–546.
141 Z. C. Dong, X. L. Zhang, H. Y. Gao, Y. Luo, C. Zhang, L. G. Chen, R. Zhang, X. Tao, Y. Zhang, J. L. Yang and J. G. Hou, *Nat. Photonics*, 2009, **4**, 50–54.
142 P. Anger, P. Bharadwaj and L. Novotny, *Phys. Rev. Lett.*, 2006, **96**, 113002.
143 S. Kühn, U. Håkanson, L. Rogobete and V. Sandoghdar, *Phys. Rev. Lett.*, 2006, **97**, 017402.
144 M. Ringler, A. Schwemer, M. Wunderlich, A. Nichtl, K. Küerzinger, T. A. Klar and J. Feldmann, *Phys. Rev. Lett.*, 2008, **100**, 203002.
145 F. Tam, G. P. Goodrich, B. R. Johnson and N. J. Halas, *Nano Lett.*, 2007, **7**, 496–501.
146 G. Wrigge, I. Gerhardt, J. Hwang, G. Zumofen and V. Sandoghdar, *Nat. Phys.*, 2007, **4**, 60–66.
147 E. C. Le Ru, P. G. Etchegoin, J. Grand, N. Félidj, J. Aubard and G. Lévi, *J. Phys. Chem. C*, 2007, **111**, 16076–16079.
148 A. V. Balatsky, Y. Manassen and R. Salem, *Phys. Rev. B: Condens. Matter*, 2002, **66**, 195416.
149 X. D. Guo, L. Dong, Y. Guo, X. Y. Shan, J. M. Zhao and X. H. Lu, *Chin. Phys. Lett.*, 2013, **30**, 17601.
150 B. Pettinger, in *Surface-Enhanced Raman Scattering*, ed. K. Kneipp, M. Moskovits and H. Kneipp, Springer, Berlin, Heidelberg, 2006, vol. 103, ch. 11, pp. 217–240.